Title
Simple device modification simultaneously enhances indoor passive evaporative cooling power and duration

Journal
Cell Reports Physical Science, 7(7)

ISSN
2666-3864

Authors
Chen, Sarah Mizuno
Kaur, Sumanjeet
Dames, Christopher Eric

Publication Date
2026-07-01

DOI
10.1016/j.xcrp.2026.103386

Cell Reports
Physical Science

Article

Simple device modification simultaneously enhances indoor passive evaporative cooling power and duration

Graphical abstract

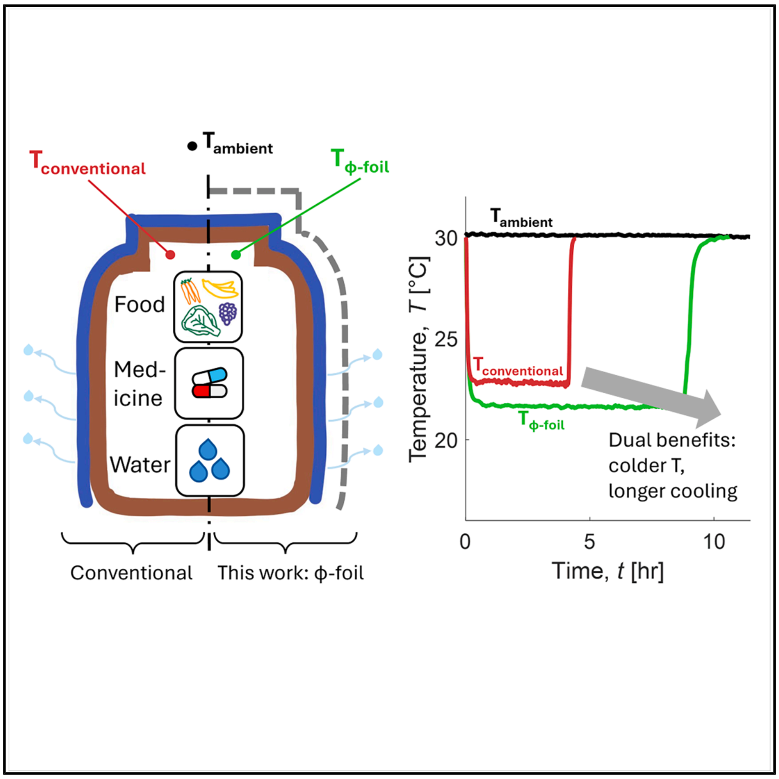

Authors

Sarah Mizuno Chen, Sumanjeet Kaur, Christopher Eric Dames

Correspondence

cdames@berkeley.edu

In brief

Chen et al. developed a perforated foil shield suspended above a stagnant airgap to enhance passive evaporative cooling for off-grid preservation of food and for cooling medicine and water. This simple addition increased the achievable temperature drop while sharply reducing water consumption.

Highlights

- Evaporative cooling is used in areas of the world that lack access to electricity
- An inexpensive, easily accessible enhancement for such cooling is demonstrated
- The device provides simultaneous wins in both cooling power and water conservation

Chen et al., 2026, Cell Reports Physical Science 7, 103386
July 15, 2026
https://doi.org/10.1016/j.xcrp.2026.103386

Cell Reports
Physical Science

Article

Simple device modification simultaneously enhances indoor passive evaporative cooling power and duration

Sarah Mizuno Chen,[1,2] Sumanjeet Kaur,[2] and Christopher Eric Dames[1,2,3,*]
[1]Department of Mechanical Engineering, University of California, Berkeley, Berkeley, CA 94720, USA
[2]Energy Technologies Area, Lawrence Berkeley National Laboratory, Berkeley, CA 94720, USA
[3]Lead contact
*Correspondence: cdames@berkeley.edu
https://doi.org/10.1016/j.xcrp.2026.103386

SUMMARY

Passive evaporative cooling from a damp cloth or vessel can be used for localized cooling of perishables such as food and medicine, drinking water, and even people. Such applications have two key objectives, which are normally in tension with each other: minimizing the water consumption rate and maximizing the cooling (steady-state temperature swing between the cool cloth and the warm surroundings). Here, we present a simple device that delivers higher performance in both metrics simultaneously by adding a perforated aluminum foil sheet suspended over a stagnant air layer to thermally shield the evaporating surface while also facilitating mass transfer. Experimental results demonstrate a simultaneous 10%–25% increase in temperature swing and 2–3× reduction in water consumption rate as compared to conventional evaporative cooling. This improvement is achieved through careful modeling to optimize the coupled heat and mass transfer through the airgap (thermally insulating and vapor permeable) and perforated foil (infrared reflective and vapor permeable).

INTRODUCTION

One in seven people globally lacks access to cooling via electricity,[1,2] and according to a UN sponsored report, this means that over 1 billion people, primarily in low-income and marginalized communities, face risks from food insecurity and health due to inadequate access to cooling, especially as climate change causes global temperatures to rise.[3] The scale of the global impact includes an estimated annual food loss exceeding 1 billion tons with a value of ~1 trillion USD. This includes over 50 countries identified as being highly impacted by a lack of access to cooling (Figure S1), and many of these populations must rely on passive methods for cooling perishables such as food and medicine as well as for personal thermal management.

Conventional evaporative cooling (see Figures 1A and 1B) has been used for centuries to passively cool perishables.[4,5,6] For example, cooling a bag of grain by an additional 5°C approximately doubles its storage lifetime,[7] and over 100,000 evaporatively cooled earthenware *zeer* pots in central Africa[8] are capable of dramatically extending the shelf life of key vegetables, from only a few days at room temperature to up to 2–3 weeks in the cooled pots.[9] Evaporative cooling through fur and hair is also important for thermoregulation of mammals,[10] including humans.[11] An important limitation, however, is that using evaporative cooling on a large scale raises the concern of water scarcity, especially in the hot, dry climates where it is most effective.

Therefore, the two key objectives in such applications are minimizing the water consumption rate while maximizing the cooling ability (e.g., as measured by the steady-state temperature difference, ΔT, between the wet cloth and the warm surroundings). These goals are generally in conflict with each other. For example, a notable recent work (Figure 1C) reduced the water consumption rate by incorporating an insulating aerogel sheet above a porous water-holding hydrogel layer.[10] This shielded evaporative cooling approach demonstrated 2×–3× water savings compared to the conventional evaporative cooling configuration of Figure 1B but with the tradeoff of a ~15% weaker cooling effect (less ΔT). There are also practical limitations when using aerogel (expensive and brittle) and hydrogel (takes hours to days to regenerate with water).

Other works[12–18] have focused on evaporative cooling in outdoor settings, most often assuming a rooftop or similar placement with a direct view of a clear sky so that the cold temperatures of deep space can be exploited as a heat sink for the thermal radiation. While such outdoor settings can substantially increase the temperature swing of an evaporative cooling device, this also raises significant practicality concerns if applied to the storage of food and other perishables because of the increased risks of outdoor exposure to pests, dust, and

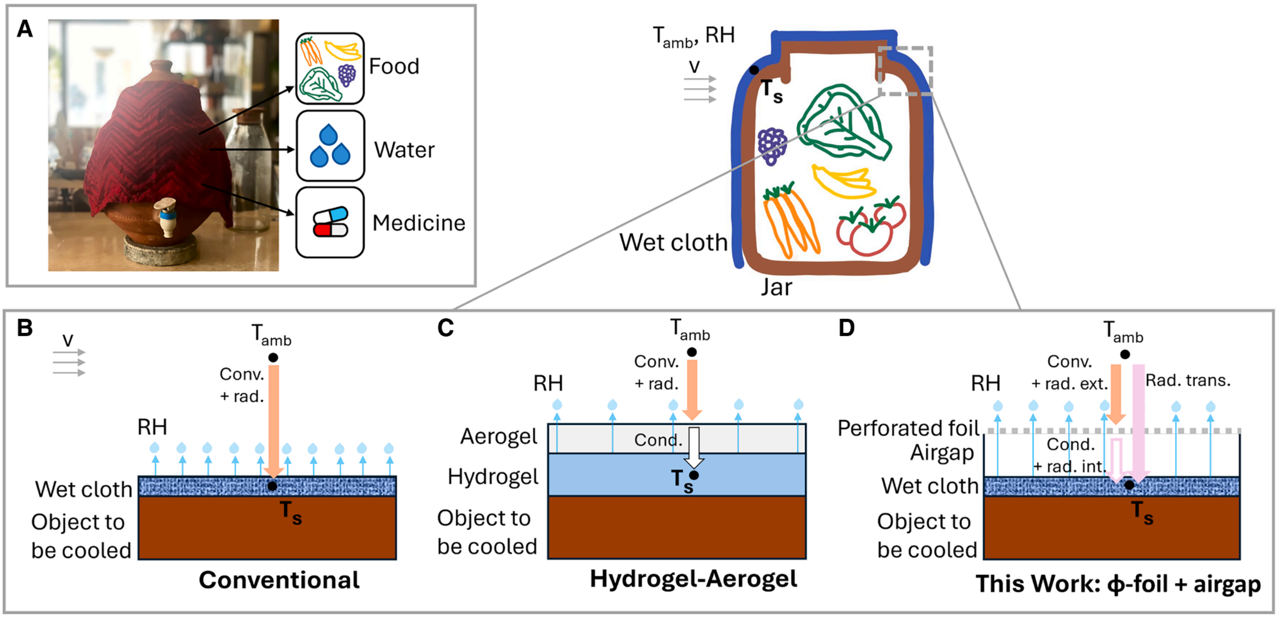

Figure 1. Introduction to passive evaporative cooling, used around the world to cool food, water, and other perishables in regions that lack access to electricity

These applications work best indoors or in otherwise shaded conditions.

(A) A traditional passive evaporative cooling jar with a damp cloth, used to extend the shelf life of food, cool water, and preserve medicines (image from Thiagarajan[4]).

(B–D) Comparison of three passive evaporative cooling concepts, each of which could be adapted to the jar indicated in (A). (B) Conventional evaporative cooling, such as the wet cloth covering the jar of food. The evaporation draws in heat from the surroundings and reduces T_s below T_{amb}. Any air movement (free-stream velocity v) makes the evaporation stronger, which is helpful for further reducing T_s but at the cost of increasing the water consumption, thereby representing an antagonistic heat- and mass-transfer tradeoff. (C) A previous work[10] reduced the water consumption by introducing a hydrogel-aerogel bilayer. The aerogel reduces the heat gain from the surroundings while also impeding the evaporation rate, resulting in a longer cooling duration at the cost of a slightly warmer T_s (weaker ΔT). (D) The concept of this work. A stagnant airgap (similar to the aerogel in C but with much easier vapor mass transfer) is created above the evaporating surface, defined by a perforated aluminum foil designed to limit external heat gains from convection and radiation while still allowing water to evaporate. This increases both cooling duration and ΔT as compared to (B).

inclement weather. Accordingly, the present work focuses on indoor settings.

Here, we present an inexpensive and simple approach to shielded evaporative cooling in indoor settings that delivers higher performance in both key metrics simultaneously, both enhancing temperature swing and reducing the water consumption rate, without the necessity of open-sky exposure on a rooftop. As shown in Figure 1D, this new design works by introducing an airgap covered by a perforated aluminum foil sheet (ϕ-foil) above the conventional evaporative cooling configuration of Figure 1B. This thermally shielded design provides additional radiative and conductive insulation against heat gain from the surroundings while still allowing water vapor to pass through, causing the evaporative cooling power to be better localized and trapped at the surface of the damp cloth. The choice of aluminum foil is due to its low cost and low emissivity, which blocks infrared (IR) radiative heat transfer from the surroundings and within the airgap (note that this is the opposite of the IR strategy for rooftop concept devices whose outermost covering is designed to transmit, rather than block, IR radiation in order to cool to deep space[12–18]). The foil can be perforated using either a needle-holding machine tool, which is precise and uniform for well-controlled experiments, or a microneedle roller, which is cheaper, faster, and more suitable for practical use (see Note S1; Figures S2 and S3).

RESULTS

Modeling framework

Conventional evaporative cooling is determined by the coupled heat and mass transfer between the wet cloth and the surrounding air,[19–21] as indicated schematically in Figure 2A. The difference in water vapor concentration (here expressed in terms of its mass density, ρ) between the saturated vapor directly above the wet cloth surface ($\rho_s = \rho_{sat}(T_s)$, where the subscript s denotes surface) and the drier surrounding ambient air ($\rho_{amb} = RH \times \rho_{sat}(T_{amb})$, where RH is the relative humidity) drives vapor diffusion away from the surface and thus induces more evaporation. Here, $\rho_{sat}(T)$ is the saturation vapor density at temperature T.

Due to water's latent heat, h_{fg}, this evaporation cools the cloth's surface, lowering T_s and thus ρ_s. This phenomenon continues until a steady state temperature difference is reached between the surface and the ambient, and the evaporation rate becomes constant. The two key performance metrics are the steady state temperature difference, $\Delta T = T_{amb}\text{-}T_s$, and the

CellPress
OPEN ACCESS

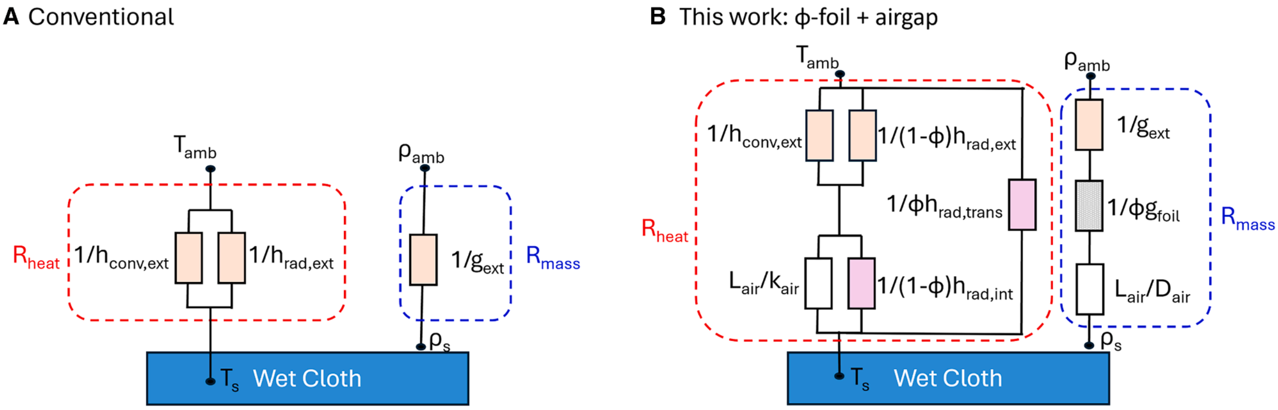

Figure 2. Heat and mass transfer resistance networks in evaporative cooling

(A) Resistance networks for conventional evaporative cooling, corresponding to Figure 1B.

(B) Resistance network for the ϕ-foil + airgap design of this work, corresponding to Figure 1D. All resistances have been normalized by the exposed face area of the wet cloth. The resistors are color-coded as follows: orange for external heat and mass transfer, white for new internal conduction/diffusion resistances, pink for new radiative resistances, and gray for the new mass transfer resistance through the perforated foil.

relative cooling duration, τ, with SI units s-m^2/kg, which is simply the inverse of the evaporation mass flux $\dot{m}''$.

We focus on steady state and initially assume no additional heat loading from the backside of the cloth (a constraint which is relaxed later, see Methods section, Figures 3A–3D below; Note S2; Figure S4). In these conditions, the well-known solution[19–21] for ΔT is found by equating the heat flux downward from the surroundings, $q''_{load} = \frac{T_{amb} - T_s}{R_{heat}}$, with the heat flux of evaporation, $q''_{evap} = h_{fg} \cdot \dot{m}''$, where $\dot{m}'' = \frac{\rho_s - \rho_{amb}}{R_{mass}}$ is the evaporation mass flux (kg/m^{2}s). This gives

$$\Delta T \equiv T_{amb} - T_s = h_{fg} \cdot \left(\frac{R_{heat}}{R_{mass}}\right) \cdot \left[\rho_{sat}(T_s) - RH \cdot \rho_{sat}(T_{amb})\right], \qquad \text{(Equation 1)}$$

where R_{heat} and R_{mass} are the area-normalized total heat and mass transfer resistances, with units m^{2}K/W and s/m, respectively. All resistors are normalized by the same area, that of the exposed top surface of the wet cloth. We evaluate the water saturation function $\rho_{sat}(T)$ using the MATLAB XSteam package.[22]

The devices in this work exhibit a nearly constant cloth temperature (see Figure 3E) and evaporation rate (see Note S3; Figure S5) for many hours. Thus, the total cooling duration, t_{cool}, scales linearly with the initial water loading m''_0, expressed as kg of water per m^2 of cloth face area. To normalize out the effect of the initial water loading, we introduce the relative cooling duration, $\tau \equiv t_{cool}/m''_0$, which is a measure of the efficiency of water consumption. Assuming a constant evaporation rate ($\dot{m}''$), this key quantity is given by

$$\tau \equiv \frac{t_{cool}}{m''_0} = \frac{1}{\dot{m}''} = \frac{R_{mass}}{\rho_{sat}(T_s) - RH \cdot \rho_{sat}(T_{amb})}. \qquad \text{(Equation 2)}$$

Because we have expressed Equations 1 and 2 in terms of the generic resistors R_{heat} and R_{mass}, these results are universally applicable to all three device configurations of Figures 1B–1D. Accordingly, the specific results for each device configuration are obtained by evaluating each of their respective R_{heat} and R_{mass} circuits and then solving Equations 1 and 2.

Beginning with conventional evaporative cooling,[19–21] referring to Figure 2A, we immediately see that its total heat transfer resistance is simply the parallel combination of external convective and radiative heat transfer coefficients, $R_{heat} = \frac{1}{h_{conv,ext} + h_{rad,ext}}$. Trivially, its total mass transfer resistance is simply the external mass transfer coefficient, $R_{mass} = \frac{1}{g_{ext}}$.

The airgap and foil configuration of the present work introduces several new components into the heat and mass transfer circuits, as seen in Figure 2B. The heat transfer now includes parallel conduction and radiation through the airgap to the foil, in parallel to radiation through the holes in the foil, giving an overall effective resistance of

$$R_{heat}^{-1} = \phi h_{rad,trans} + \left[\left((1-\phi)h_{rad,int} + k_{air}/L_{air}\right)^{-1} + \left(h_{conv,ext} + (1-\phi)h_{rad,ext}\right)^{-1}\right]^{-1}, \qquad \text{(Equation 3)}$$

where ϕ is the foil open area fraction, L_{air} is the airgap thickness, and k_{air} is the air thermal conductivity. Note that because the device operates indoors, we have treated the convection and radiation as both having the same external T_{amb}.

Similarly, the mass transfer resistance for the ϕ-foil + airgap configuration adds additional resistance due to the airgap and the foil:

$$R_{mass} = \frac{L_{air}}{D_{air}} + \frac{1}{\phi g_{foil}} + \frac{1}{g_{ext}}, \qquad \text{(Equation 4)}$$

where D_{air} is the mass diffusivity of water vapor in air.

For both heat and mass transfer, the airgap is treated as a stagnant air layer rather than as convection (this is well justified, see Notes S4–S6; Figure S6). All components in these heat and mass transfer circuits were determined independently through a combination of literature and other auxiliary experiments (see Notes S7 and S8; Figure S7; Tables S1 and S2 for more details).

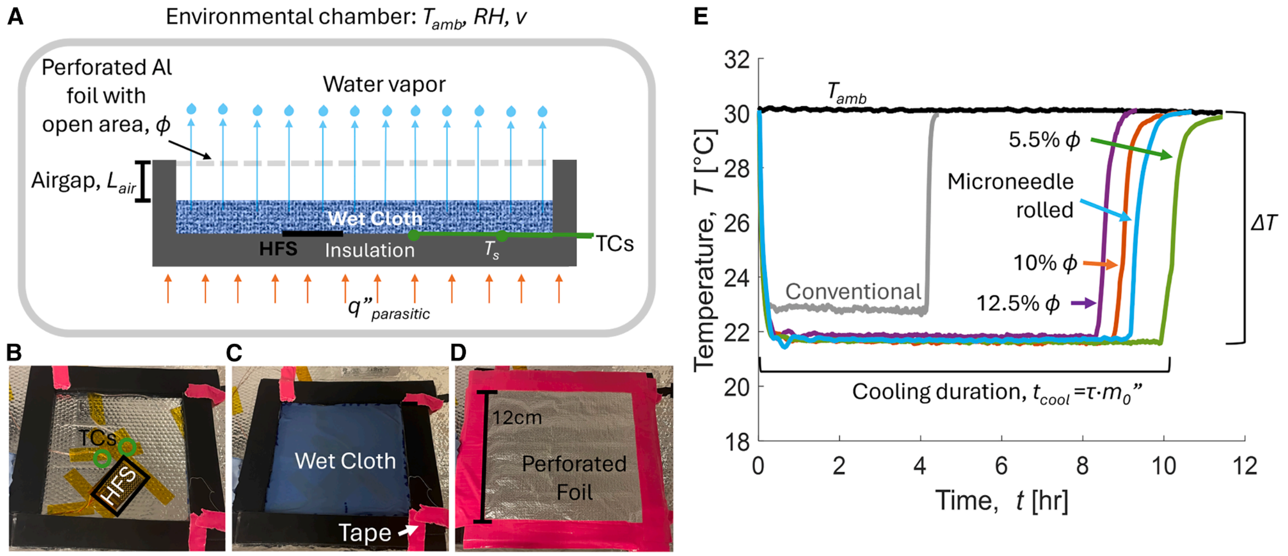

Figure 3. Benchmark horizontal cooling experiments

Experimental setup (A–D) and representative cooling curve results (E) for varying foil perforation. (A) Side view schematic, including the possibility of parasitic heat loading $q''_{parasitic}$ from the back side. TCs, thermocouples and HFS, heat flux sensor. (B–D) Series of the top-view photographs showing sequential steps in assembling the device. (B) View of the thermocouples and HFS on top of the insulation. (C) After placing the wet cloth. (D) Final configuration after placing the perforated foil. The bright pink and translucent brown strips in (B–D) are pieces of tape used to secure various wires and the top foil. (E) Experimental cooling curves show the effects of varying foil perforation ϕ on the cooling performance of the ϕ-foil device (colored curves) as compared to conventional evaporative cooling (gray curve). L_{air} is fixed at 6 mm with v = 0.10 m/s, T_{amb} = 30°C, RH = 40%, and m''_0 = 0.42 kg/m^2.

Finally, using Equations 1 and 2, we can predict temperature swing and cooling duration with no free parameters.

Benchmark horizontal cooling tests

The present device has two key design parameters: the open area fraction of the perforated foil, ϕ, and the airgap thickness, L_{air}. We explored these effects both experimentally (Figures 3A–3D and Methods section) and theoretically (Figure 2) through a series of devices of varying ϕ and L_{air} (Figures 3E and 4). Figure 3E shows a representative measured cooling curve for the conventional evaporative cooling configuration (corresponding to the schematic of Figure 1B) in gray, as compared to cooling curves for four ϕ-foil + airgap devices (schematic of Figure 1D) with varying foil perforation. The colored lines in Figure 3E show that ϕ-foil + airgap enhances *both* ΔT and t_{cool} for all tested foils. The effects on t_{cool} are pronounced, as it has more than doubled for all foils. Figure 3E also shows that ΔT in these devices has increased by more than 1°C compared to the conventional approach. Microscopy shows no evidence of salt accumulation on the foil with the use of tap water (see Figure S8).

Next, Figures 4A and 4B summarize at a higher level the Figure 3E results for t_{cool} and ΔT as functions of ϕ, all for fixed L_{air}. Model curves with no free parameters are also included (blue lines, using the model from Note S2, which augments Equations 1, 2, 3, and 4 with the modest backside $R_{parasitic}$), demonstrating excellent agreement with the experiments. For reference, the results for the conventional evaporative cooling device are depicted by the gray lines. The results for the microneedle rolled foil of Figure 3E cannot be plotted in Figures 4A and 4B because the foil perforation is not well known, though its ϕ can be estimated to be around 8%–9% based on where that sample's data falls in Figure 3E between the ϕ = 5.5% and 10% foils.

Similarly, Figures 4C and 4D show experimental and modeling results for varying L_{air} with fixed ϕ. The data in Figures 4C and 4D spans over 50 h of testing with tap water. Again, there is excellent agreement between model and experiment, across all 50 h of testing on the same foil, with no free parameters.

Thinking physically about the trends of Figure 4, we note that increasing L_{air} increases both R_{heat} and R_{mass}, the latter of which directly increases t_{cool} (Figure 4C; Equation 2). On the other hand, when considering ΔT we see from Equation 1 that the heat and mass transfer resistances have competing effects (see Note S9 and Figure S9), and either might dominate in different regimes of L_{air} depending on the contributions of the other terms to Equations 3 and 4, as discussed further below with Figure 5. Note that the device with nominally zero L_{air} corresponds to the foil being placed directly on top of the wet cloth, i.e., direct contact with no spacer or scrim to hold a small gap. In practice, we believe the residual airgap for this nominal "direct contact" condition to be in the range $0 \leq L_{air} \lesssim 300$ μm, the uncertainty of which has essentially no practical effect on the model or experiment (see Note S9). The thermal circuit of Figure 2B and the corresponding model of Equation 3 are both smooth and continuous with respect to L_{air}, including in the limit $L_{air} \rightarrow 0$, so that in both model and experiment we confirm that there are no step function artifacts related to the foil potentially being in direct contact with the cloth.

Another metric for a limited-time cooling device like this is its "°C-hour cooling," which captures the combined effects of both ΔT and cooling duration by multiplying them. This is closely

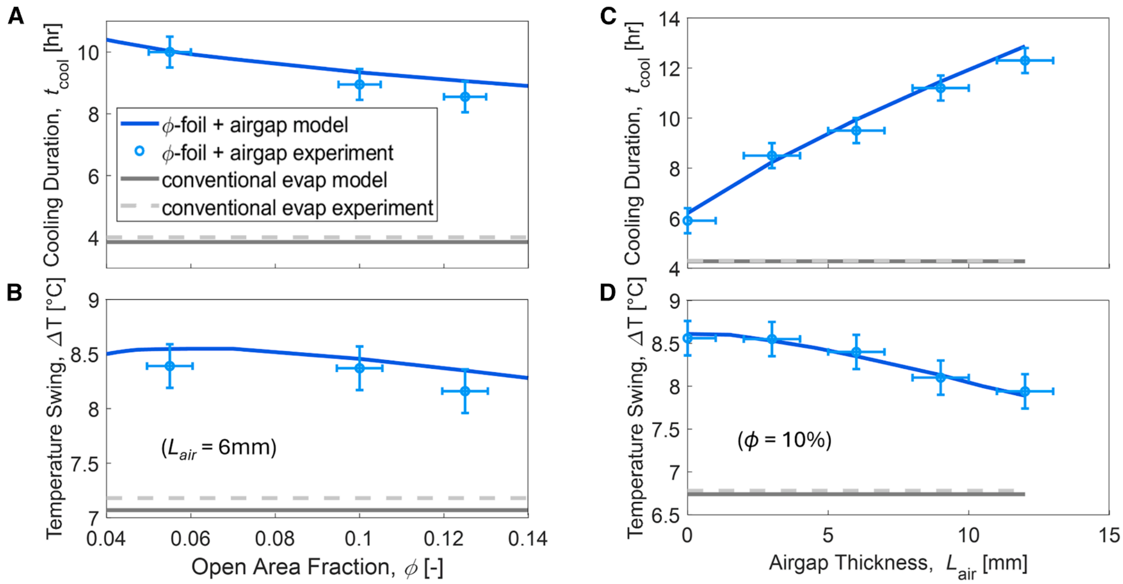

Figure 4. Summary of the key performance metrics t_{cool} and ΔT when varying the two main design parameters ϕ and L_{air}

(A) and (B) vary ϕ with fixed L_{air} and, similarly, (C) and (D) vary L_{air} with fixed ϕ. Points in (A) and (B) were obtained by analyzing the raw cooling curve data from Figure 3E and, similarly, the points in (C) and (D) from analogous $T(t)$ cooling curve data. (A) Summary of t_{cool} as a function of ϕ for the three devices from Figure 3E with well-characterized ϕ (points), along with the model with no free parameters (solid lines). For comparison, t_{cool} for the conventional configuration of Figure 1B is indicated by the gray lines for the corresponding measurement (light gray, dashed) and model (darker gray, solid). (B) The analogous summary of the ΔT results. Similarly, (C) and (D) are analogous to (A) and (B) but for varying L_{air} at fixed ϕ. Other experimental parameters for all panels are T_{amb} = 30°C, RH = 40%, and m_0'' = 0.42 kg/m^2, with v = 0.10 m/s in (A) and (B) and 0.07 m/s in (C) and (D). Error bars are ±0.2°C (average standard deviation between two thermocouple readings) for ΔT, ±0.5 h (average time taken to go from T_{amb} to T_s at the start of experiments) for t_{cool}, and ±0.5% (average standard deviation over four measured hole areas) for ϕ and ±1 mm (ruler measurement limit) for L_{air}.

related to the concept of "cooling-degree days" used in analyzing air conditioning demand. Referring to Figure 3E, the best performing device had 5.5% open area foil with a 6-mm airgap (green curve). Compared to the conventional evaporative cooling configuration (gray curve in Figure 3E), this best device gave a 2.5× increase in cooling duration and 17% increase in the cooling ΔT, which together give a 2.5 × 1.17 = 2.9× increase in the °C-hour cooling (for comparison, the previous

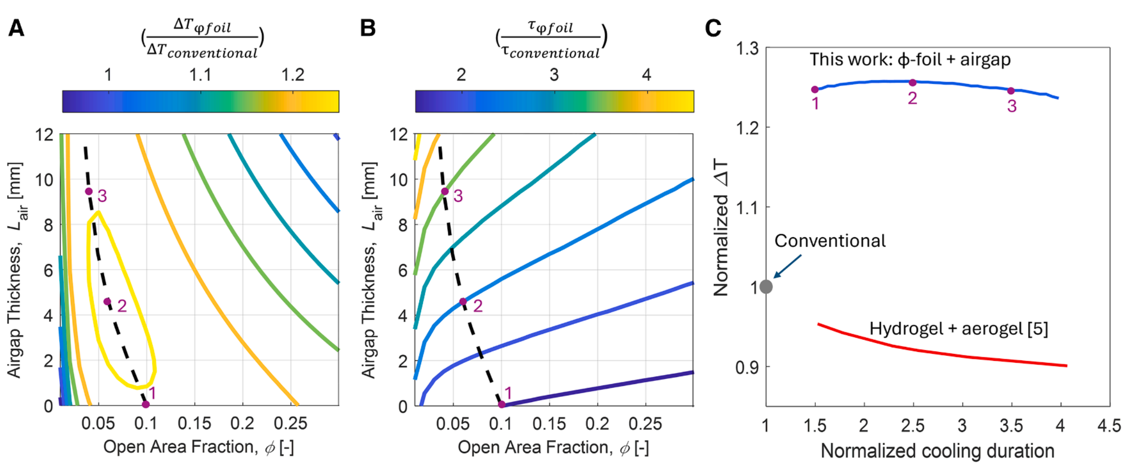

Figure 5. Parametric modeling of the ϕ-foil + airgap design

(A) Effects of ϕ and L_{air} on ΔT, expressed on a normalized basis as compared to ΔT for conventional evaporative cooling.

(B) Similar model results for cooling duration, again on a normalized basis.

(C) Pareto curve of the normalized ΔT and τ for this work, along with the corresponding Pareto curve for a previous cooling enhancement device using hydrogel and aerogel.[10] The purple points 1, 2, and 3 on (A) and (B) lie on the line of maximum normalized ΔT for a given normalized τ, which is also depicted in (C). For all results in this figure T_{amb} = 30°C, RH = 40%, and v = 0.10 m/s.

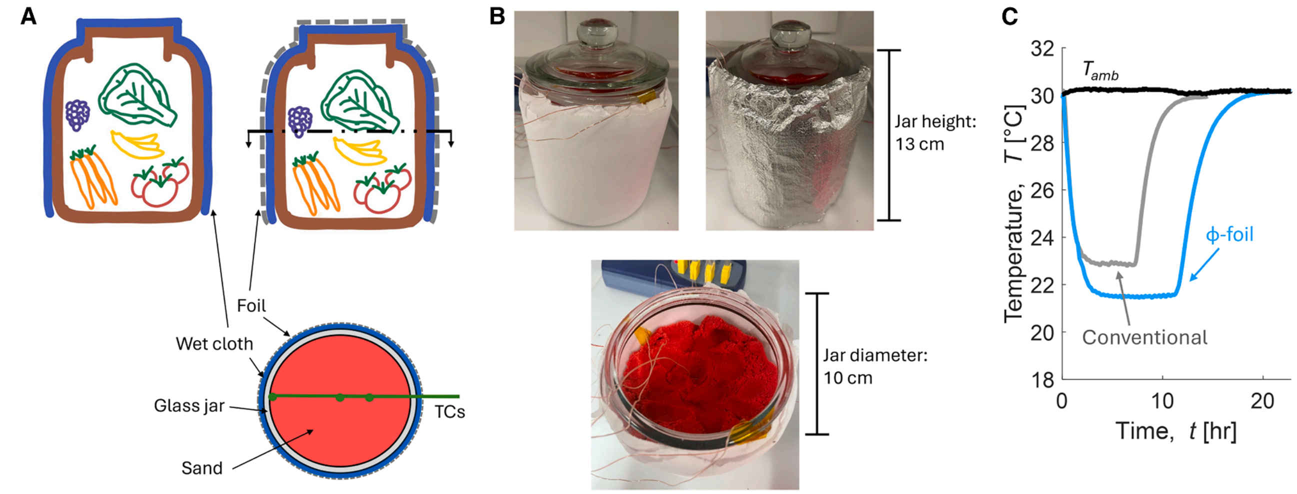

Figure 6. Experiments mimicking the real-life use case of indoor evaporative cooling for preserving perishable foodstuffs in a jar

(A) Schematic of the experimental setup and relation to Figure 1A, with sand (red) representing the thermal mass of a stored perishable. The lower schematic represents a cross-section at the indicated mid-plane.

(B) Photographs corresponding to the diagrams in (A).

(C) Experimental cooling curves (average of the three thermocouples from (A)) for the sand thermal mass within the glass jar. Note: for the blue curve, the foil was added after 1.5 h to demonstrate the immediate ΔT boost. (In these trials, T_{amb} = 30°C, RH = 40%, v = 0.07 m/s, and m''_0 = 1 kg/m^2 water loading).

hydrogel-aerogel device[10] reported a 2.5× increase in °C-hour cooling as compared to the conventional configuration).

We also have extended this study to consider the performance when a substantial heat load is applied to the backside, by inserting a joule heating sheet between the wet cloth and the insulation, equivalent to a prescribed $q''_{parasitic}$ in the schematic of Figure 3A. The results for ΔT as a function of the heat load are given in Notes S10–S12 and Figures S10–S13, with excellent agreement between model and experiment, and the present device again outperforms conventional evaporative cooling for heat loads up to 60 W/m^2.

Parametric modeling

Having validated the heat and mass transfer model against experiments in Figures 4, S5, and S10, we now use the model to analyze a broader range of the principal design parameters, ϕ and L_{air}. We continue to emphasize the key performance metrics ΔT and τ, here focusing on their dimensionless values as normalized to conventional evaporative cooling under the same external conditions, and all assuming no parasitic heat gain or applied heat load.

Figures 5A and 5B show the results of these model parametric sweeps. Figure 5A shows that this relative ΔT (colored contours) is maximized for an intermediate range of L_{air} and ϕ. For example, see the yellow contour which covers from around L_{air} ∼1–8 mm and ϕ ∼5%–10%. Figure 5B, on the other hand, shows a purely monotonic dependence of the relative cooling duration on both design variables; the cooling time is always extended by reducing the foil porosity and/or increasing the airgap thickness, which makes sense because both increase the overall mass transfer resistance.

Finally, we merge the information from Figures 5A and 5B into a single Pareto curve in Figure 5C. This represents the optimal frontier of the maximum ΔT that could be achieved for a given τ, and equivalently, the maximum τ that could be achieved for a given ΔT, by choosing the corresponding optimal values of (ϕ, L_{air}), such as the three purple points from Figures 5A and 5B marked 1–3. This optimal frontier in Figure 5C has a nearly constant ΔT, yet the relative cooling duration can be greatly increased from 1.25 to 4 (following along the marked points from 1 to 3) with only a minimal reduction in ΔT.

For comparison, Figure 5C also shows the equivalent pareto tradeoff curve for the model from the previous aerogel/hydrogel work (where $R_{heat} = \frac{1}{h_{conv,ext}+h_{rad,ext}} + \frac{L_{aero}}{k_{aero}}$ and $R_{mass} = \frac{1}{g_{ext}} + \frac{L_{aero}}{D_{aero}}$, using material property values from Lu et al.[10]); while that approach could also achieve major gains in the cooling duration, it came with an antagonistic reduction in ΔT as compared to conventional evaporative cooling.

Demonstration in a jar with thermal mass

We conclude the experimental results with a demonstration closer to the real-life use case of a jar with perishables (as in Figure 1A). A glass jar was filled with kinetic sand as a thermal mass representing the perishable to be cooled, and wrapped in a wet cloth covered by ϕ-foil, as indicated in Figures 6A and 6B. Three fine-gauge thermocouples were embedded within the sand.

Revising the heat and mass transfer model in light of the vertical nature of the jar surface because that makes the external natural convection non-negligible (see Notes S5 and S13; Figure S14), the model indicates that the best performance is expected for airgaps of 0–10 mm, and moderate open area fractions of ∼10%–20%. We therefore used a microneedle rolled foil with ∼2× perforation density of that from Figure 3E with its estimated ϕ of 8%–9%, giving an estimated ϕ of 16%–18%, and we wrapped it closely around the underlying cloth, corresponding to an airgap of less than 1 mm. To demonstrate the impact of the ϕ-foil approach, we compared it directly to measurements in the conventional configuration for the same jar wrapped with just a wet cloth alone.

The measurement results in Figure 6C show several interesting features. The equilibration time to reach steady state is now over 1 h, much longer than in the previous experiments, due to the additional thermal mass of the sand. Most importantly, comparing the blue (ϕ-foil) and gray (conventional configuration) device results in Figure 6C, we again see a simultaneous increase in temperature swing (by about 20%) and cooling duration (by about 50%) with the addition of the foil, demonstrating the real-life potential of this work.

DISCUSSION

We now consider the fundamental drivers and ultimate limits of simultaneous ΔT and τ enhancement in shielded evaporative cooling for indoor settings. Table 1 puts these fundamental quantities in context across a variety of designs, including their theoretical limits as well as summarizing what has been achieved in practice. Focusing on a fixed environmental T_{amb} and RH (see Note S14; Figures S15 and S16 for effect of T_{amb} and RH), the dominant effect on τ is easily seen in Equation 2: increasing R_{mass} tends directly to extend τ (although there are also second-order effects via the $\rho_{sat}(T_s)$ term, which couples with Equation 1). Similarly, Equation 1 shows that ΔT is driven by both R_{heat} and R_{mass}, though importantly, they emerge tied together as the *ratio* R_{heat}/R_{mass}.

The first three rows of the table deal with conventional evaporative cooling, in which the free-stream airspeed v can play a major role (see Notes S15 and S16 and Figures S17 and S18). Regardless of the orientation (horizontal and vertical) and convective regime (natural and forced), the heat and mass transfer boundary layer analogies[19,23] apply and thus $h_{conv,ext}$ and g_{ext} are linearly related by:

$$\frac{g_{ext}}{h_{conv,ext}} = \frac{D_{air}}{k_{air}} \cdot Le^n, \qquad \text{(Equation 5)}$$

where Le is the Lewis number (0.85 for water vapor in air at room temperature), and the exponent n ranges from 1/3 to 1/4; there is virtually no practical difference between $Le^{1/3}$ and $Le^{1/4}$. Thus, for air, the ratio $\frac{g_{ext}}{h_{conv,ext}} = 9.1 \times 10^{-4}$ m^3K/J at room temperature, regardless of the convective regime, leading to an important theoretical limit in conventional evaporative cooling as seen in row 1 of the table. It is clear (Figure 2A; Equation 1) that ΔT is maximized when radiation is negligible, in which case, $\frac{R_{heat}}{R_{mass}}$ goes from $\frac{g_{ext}}{h_{conv,ext}+h_{rad,ext}}$ to simply $\frac{g_{ext}}{h_{conv,ext}}$, and thus $\approx 9.1 \times 10^{-4}$ m^3K/J from Equation 5. For the reference scenario of T_{amb} = 30°C and RH = 40%, the corresponding theoretical maximum ΔT = 10.2°C.

Row 2 is a more practical limit of forced conventional evaporative cooling for strong but finite $h_{conv,ext}$ and non-negligible $h_{rad,ext}$, approximating the wet bulb temperature.[24,25] In practical passive evaporative cooling (row 3), however, airspeeds are low and the relative influence of radiation is larger, resulting in a reduced $\frac{R_{heat}}{R_{mass}}$, and therefore under these conditions, ΔT = 7.1°C, as seen in Figure 4.

Turning to shielded evaporative cooling, we first consider the ideal properties of the insulating layer (e.g., aerogel and air) above the damp cloth. As the thickness of this layer becomes sufficiently large, the ratio R_{heat}/R_{mass} tends to D/k. Thus, it is the *ratio* between vapor diffusivity and thermal conductivity, rather than either property in isolation, that is the most important factor in determining ΔT. Even though aerogel has an outstandingly small k, even below k_{air}, its microstructure also impedes vapor flow, and aerogel's D/k ratio is over three times worse than that of air (compare rows 4 and 5). Thus, in this ideal limit (which in principle might be approached with ϕ-foil using a double foil layer with staggered holes to completely block direct IR transmission or a single layer with ~1 μm sized holes, see Note S17), R_{heat}/R_{mass} for passive shielded evaporative cooling using an air layer has >3× the R_{heat}/R_{mass} of aerogel, and even surpasses the theoretical limit for forced conventional evaporative cooling (compare rows 5, 4, and 1). Because the hole diameters in these ϕ-foil designs are around 200 μm and greater, the heat and mass transfer physics remain solidly in the classical, continuum regimes. However, if much smaller holes were considered with diameters approaching ~10 μm, several additional subcontinuum transport phenomena should also be considered (see Note S17).

Despite air having a highly favorable D/k ratio for enhancing evaporative cooling, unlike aerogel, it also has the major shortcoming of transmitting IR thermal radiation. Thus, a vital part of the present research is incorporating the perforated aluminum foil and the joint optimization of its radiative and mass-transfer properties. Comparing the experimental results in rows 3 and 6 shows that the ϕ-foil + airgap design is the highest performing, both in terms of the fundamental cooling metrics R_{heat}/R_{mass} and ΔT, as well as R_{mass} individually, which drives the water usage efficiency (see Note S18; Table S3 for comparison to modeled aerogel/hydrogel and further discussion).

Finally, we identify an ultimate theoretical limit to any shielded evaporative cooling (row 7) by considering $R_{heat}/R_{mass} \rightarrow \infty$ in Equation 1. Since ΔT must remain finite, $\rho_{sat}(T_s)$ must equal $RH \times \rho_{sat}(T_{amb})$, which yields a theoretical minimum value for T_s. This is simply the dew point. For the selected reference scenario, this gives a theoretical ΔT limit of 15.9°C.

The main focus of this paper is evaporative cooling in an indoor environment, where storage of cooled perishables is likely to be most practical due to the shelter from pests, contaminants, and inclement weather. In Note S19 and Table S4, we also comment on how this ϕ-foil design is expected to perform in several types of outdoor environments. Besides the hydrogel + aerogel device of Lu et al.,[10] which was only analyzed for a shaded indoor setting, another somewhat related work on shielded evaporative cooling is Yu et al.[13] for a hydrogel + air layer + porous polyethylene film device. A major difference, however, is that the latter is intended for outdoor use with a direct view of a clear sky, which means it must manage the solar load and also can exploit the cold temperature of deep space as an IR heat sink; thus, the polyethylene film in Yu et al.[13] is chosen for high IR transmissivity to *maximize* IR heat exchange. This is the opposite of what is required for indoor cooler applications like the present ϕ-foil

Table 1. Summary of ideal limits and practically achievable values for various approaches to indoor evaporative cooling, both conventional (rows 1–3) and shielded (rows 4–7)

Row		Design configuration	Convection $h_{conv,ext}$ (W/m^{2}K)	Radiation $h_{rad,ext}$ (W/m^{2}K)	R_{mass} (s/m)	R_{heat}/R_{mass} (10^{-4} m^{3}K/J)	ΔT in ref. scenario (T_{amb} = 30°C, RH = 40%)
1	conventional	ideal limit of strongly forced convective evaporation	→∞	N/A	→0	$\frac{g_{ext}}{h_{conv,ext}} = 9.1$	10.2°C
2		practical, in forced air (same as wet bulb *T*)	~25	5.2	45	$\frac{g_{ext}}{h_{conv,ext}+h_{rad,ext}} = 7.6$	9.5°C
3		practical, passive evaporation (Figure 4)	~4	5.2	275	$\frac{g_{ext}}{h_{conv,ext}+h_{rad,ext}} = 3.6$	7.1°C[a]
4	shielded	aerogel shielded [Lu et al.[10]], ideal limit (infinitely thick aerogel)	N/A	N/A	→∞	$\frac{D_{aero}}{k_{aero}} = 3.0$	6.3°C
5		ϕ-foil and air shielded, ideal limit (infinitely thick airgap)	N/A	N/A	→∞	$\frac{D_{air}}{k_{air}} = 9.6$	10.4°C
6		ϕ-foil and air shielded, practical (Figure 4) (L_{air} = 6 mm, ϕ = 0.1)	~4	<0.5	550	$\frac{R_{heat}}{R_{mass}} = 6.1$	8.4°C[a]
7		ultimate theoretical limit (same as cooling to dew point *T*)	N/A	N/A	→∞	$\frac{R_{heat}}{R_{mass}} \rightarrow \infty$	15.9°C

N/A, not applicable.
[a]Experimental results (rows 3 and 6). See Note S18 for the expanded version of this table.

device and Lu et al.,[10] which need to minimize IR loading from the warmer surroundings.

We designed and demonstrated an inexpensive, easily fabricated enhancement for indoor shielded evaporative cooling by introducing a stagnant airgap layer held in by a perforated aluminum foil. This design synergistically increases both cooling duration and temperature swing, thereby overcoming their longstanding antagonistic tradeoff.[10] By minimizing radiation exchange with the surroundings (opposite of some other approaches that work best outdoors with a clear view to deep space[12–18]), the present design is well suited for use indoors or in similarly sheltered locations, which is advantageous for reducing exposure to weather, contaminants, and animals when preserving perishables like food, water, or medicine.

While the present work has focused on applications with negligible steady-state heat load from the cooled object, such as keeping perishables cool, the ϕ-foil and airgap approach is also beneficial for situations that require dissipating a modest heat load, like cooling of the human body in extreme heat weather events[26,27] (see Notes S10–S12). Future work could explore the ϕ-foil approach for such thermal management applications, as well as pursue more fundamental design strategies to better approach the $R_{heat}/R_{mass} \rightarrow \infty$ dew point theoretical limit.

METHODS

Experimental setup for benchmark horizontal cooling tests

The benchmark horizontal experiments were conducted in the setup shown in Figure 3A (similar to Lu et al.[10]). All measurements were performed in an environmental chamber (Electro-Tech Systems 5532) with controlled temperature and relative humidity, held at T_{amb} = 30 ± 0.2°C and RH = 40% ± 5%. The T_{amb} and RH were also independently verified using two thermo-hygrometers (HOBO MX1101). The air speed inside the chamber was also adjustable and was held at v = 0.07 m/s or v = 0.10 m/s (measured using a TESTO hot wire anemometer), an acceptable range to represent typical non-ventilated indoor air conditions[28] (Notes S20 and S21; Figure S19).

The following device assembly steps were also performed inside the environmental chamber. The initial water mass loading was m_0 = 6.0 grams of tap water (measured by a mass balance), added to a 12 cm by 12 cm polyester cloth (1 mm thick, Barcelonetta, dry fit material), corresponding to m''_0 = 0.42 kg/m^2 initial water loading (Figure 3C). The perforated foil (fabrication details in Note S1; Figures S2 and S3, characterization details in Notes S7 and S8; Figure S7; Tables S1 and S2) was then added immediately (Figure 3D), followed by a temporary vapor impermeable cover (not shown in Figure 3), which was used to allow the device to come to uniform thermal equilibrium with T_{amb} (~30–60 min) while still retaining the initial water loading. To start the test, the temporary vapor barrier cover was removed, establishing time t = 0. The cloth temperature T_s was recorded continually as the average of the two thermocouples (TCs) depicted in Figures 3A and 3B. Each test continued until all water was evaporated, which was identified by T_s returning very close to T_{amb} (within 0.2°C).

We conducted experiments for conventional evaporative cooling as the baseline comparison in the same manner, without the foil and side insulation. We used measurements from the heat flux sensor (HFS) to infer the value of an $R_{parasitic}$ (see Note S2) that accounts for the modest parasitic heat gain through the backside of the insulation, denoted $q''_{parasitic}$ in Figure 3A and found to correspond to no more than 15% of the direct heat flow through the topside of the device.

RESOURCE AVAILABILITY

Lead contact

Further information and requests for resources should be directed to and will be fulfilled by the lead contact Christopher Eric Dames (cdames@berkeley.edu).

Materials availability

This study did not generate new, unique reagents.

Data and code availability

- All data reported in this paper will be shared by the lead contact upon request.
- This paper does not report original code.
- Any additional information required to reanalyze the data reported in this paper is available from the lead contact upon request.

ACKNOWLEDGMENTS

This work is dedicated to the memory of Sumanjeet Kaur, who passed away during the final stages of the review process. We are deeply grateful for her commitment to impactful science, spirited collaboration, and supportive mentoring.

Funding for this work was provided by the Graduate Research Fellowships Program of the United States National Science Foundation as well as by the Building Technologies Program of the United States Department of Energy under contract no. DE-AC02-05CH11231.

AUTHOR CONTRIBUTIONS

Conceptualization, S.M.C.; methodology, S.M.C.; investigation, S.M.C.; writing – original draft, S.M.C.; writing – review and editing, S.M.C. and C.E.D.; resources, S.K.; funding acquisition, S.K. and S.M.C.; and supervision, C.E.D.

DECLARATION OF INTERESTS

The authors declare no competing interests.

SUPPLEMENTAL INFORMATION

Supplemental information can be found online at https://doi.org/10.1016/j.xcrp.2026.103386.

Received: February 10, 2026
Revised: April 13, 2026
Accepted: May 21, 2026
Published: July 2, 2026

REFERENCES

1. Smith, G., and Atherton, M. (2022). 1 in 7 people globally currently at high risk due to lack of access to cooling. Sustain. Energy. https://www.seforall.org/press-releases/1-in-7-people-globally-currently-at-high-risk-due-to-lack-of-access-to-cooling.
2. Dean, B., Garcia, R., Hamilton, I., Hartley, B., Jose, A., Mehic, S., Pasqualetto, G., Uwamaliya, A., and Wadhwa, A. (2022). Chilling Prospects: Tracking Sustainable Cooling for All. Sustain. Energy.
3. Abdelaziz, O., Gluckman, R., Hamilton, I., Khosla, R. & Riahi, L. Global Cooling Watch 2025. https://doi.org/10.59117/20.500.11822/48926.
4. Thiagarajan, K. (2024). As Temperatures in India Break Records, Ancient Terracotta Air Coolers Are Helping Fight Extreme Heat (BBC).
5. Verploegen, E., and Mangino, M. (2021). Clay Pot Coolers: Keep Produce Fresh without Electricity (MIT D-Lab). https://d-lab.mit.edu/news-blog/blog/clay-pot-coolers-keep-produce-fresh-without-electricity.
6. (2019). Evaporative Cooling for Fruit and Vegetable Storage in Rwanda and Burkina Faso (Feed the Future Innovation Lab for Horticulture). https://horticulture.ucdavis.edu/information/evaporative-cooling-fruit-and-vegetable-storage-rwanda-and-burkina-faso.
7. Hurburgh, C. (2019). Cooling Grain Impacts on Grain Quality and Shelf-Life (Iowa State University Extension and Outreach Integrated Crop Management). https://crops.extension.iastate.edu/post/cooling-grain-impacts-grain-quality-and-shelf-life.
8. Strauss, G. (2016). No Electricity? A Low-Tech System Keeps Things Chilled (National Geographic).
9. Odesola, I., and Onyebuchi, O. (2009). A Review of Porous Evaporative Cooling for the Preservation of Fruits and Vegetables. Pac. J. Sci. Technol. *10*, 935–941.
10. Lu, Z., Strobach, E., Chen, N., Ferralis, N., and Grossman, J.C. (2020). Passive sub-ambient cooling from a transparent evaporation-insulation bilayer. Joule *4*, 2693–2701. https://doi.org/10.1016/j.joule.2020.10.005.
11. Lasisi, T., Smallcombe, J.W., Kenney, W.L., Shriver, M.D., Zydney, B., Jablonski, N.G., and Havenith, G. (2023). Human scalp hair as a thermoregulatory adaptation. Proc. Natl. Acad. Sci. *120*, e2301760120. https://doi.org/10.1073/pnas.2301760120.
12. Li, J., Wang, X., Liang, D., Xu, N., Zhu, B., Li, W., Yao, P., Jiang, Y., Min, X., Huang, Z., et al. (2022). A tandem radiative/evaporative cooler for weather-insensitive and high-performance daytime passive cooling. Sci. Adv. *8*, eabq0411. https://doi.org/10.1126/sciadv.abq0411.
13. Yu, L., Huang, Y., Zhao, Y., Rao, Z., Li, W., Chen, Z., and Chen, M. (2024). Self-sustained and Insulated Radiative/Evaporative Cooler for Daytime Subambient Passive Cooling. ACS Appl. Mater. Interfaces *16*, 6513–6522. https://doi.org/10.1021/acsami.3c19223.
14. Galib, R.H., Tian, Y., Dang, S., Li, X., Yudhanto, A., Lubineau, G., and Gan, Q. (2023). Atmospheric-moisture-induced polyacrylate hydrogels for hybrid passive cooling. Nat. Commun. *14*, 6707. https://doi.org/10.1038/s41467-023-42548-0.
15. Lu, Z., Leroy, A., Zhang, L., Patil, J.J., Wang, E.N., and Grossman, J.C. (2022). Significantly enhanced sub-ambient passive cooling enabled by evaporation, radiation, and insulation. Cell Rep. Phys. Sci. *3*, 101068. https://doi.org/10.1016/j.xcrp.2022.101068.
16. Hu, Z., Qiu, Y., Zhou, J., and Li, Q. (2024). Smart Flexible Porous Bilayer for All-Day Dynamic Passive Cooling. Small Sci. *4*, 2300237. https://doi.org/10.1002/smsc.202300237.
17. Du, Y., Chen, Y., Yang, X., Liu, J., Liang, Y., Chao, Y., Yuan, J., Liu, H., Zhou, Z., and Yan, J. (2024). Hybrid passive cooling: towards the next breakthrough of radiative sky cooling technology. J. Mater. Chem. A. *12*, 21490–21514. https://doi.org/10.1039/D4TA03122A.
18. Tang, H., Guo, C., Zhao, X., Fan, F., Lu, R., and Zhao, D. (2025). Guidance for combining radiative cooling and evaporative cooling: A heat and mass transfer analysis. Energy Convers. Manag. *325*, 119385. https://doi.org/10.1016/j.enconman.2024.119385.
19. Bergman, T., Lavine, A., Incropera, F., and Dewitt, D. (2011). Fundamentals of Heat and Mass Transfer (John Wiley & Sons, Inc.).
20. Lewis, W.K. (1922). The evaporation of a liquid into a gas. Mech. Eng. *44*, 325–332.

21. Bird, B., Stewart, W., and Lightfoot, E. (2002). Transport Phenomena (John Wiley & Sons, Inc.).
22. Holmgren, M. X Steam, Thermodynamic properties of water and steam.
23. Lienhard IV, J., and Lienhard, V.,J. (2020). A Heat Transfer Textbook (Phlogiston Press).
24. Legg, R. (2017). Air Conditioning System Design (Butterworth-Heinemann).
25. Temperatures Including Dry Bulb/Wet Bulb/Dew Point/Potential/Equivalent Potential. weather.gov https://www.weather.gov/source/zhu/ZHU_Training_Page/definitions/dry_wet_bulb_definition/dry_wet_bulb.html.
26. Luber, G., and McGeehin, M. (2008). Climate Change and Extreme Heat Events. Am. J. Prev. Med. *35*, 429–435. https://doi.org/10.1016/j.amepre.2008.08.021.
27. Dahl, K., Licker, R., Abatzoglou, J.T., and Declet-Barreto, J. (2019). Increased frequency of and population exposure to extreme heat index days in the United States during the 21st century. Environ. Res. Commun. *1*, 075002. https://doi.org/10.1088/2515-7620/ab27cf.
28. Matthews, T., Thompson, C. & Wilson, D. Air velocities inside domestic environments: an important parameter for passive monitoring. (1987).